International Journal of Heat and Fluid Flow 30 (2009) 339–355

Contents lists available at ScienceDirect

International Journal of Heat and Fluid Flow

journal homepage: www.elsevier.com/locate/ijhff

# Characterization of fan spray atomizers through numerical simulation

Mireia Altimira *, Alejandro Rivas, Gorka S. Larraona, Raul Anton, Juan Carlos Ramos

*Thermal and Fluids Engineering Division, Mechanical Engineering Department, Tecnun (University of Navarra), Manuel de Lardizábal 13, 20018 San Sebastián, Spain*

ARTICLE INFO

*Article history:*
Received 18 July 2008
Received in revised form 3 December 2008
Accepted 15 December 2008
Available online 19 January 2009

*Keywords:*
Fan spray atomizers
Atomization
Liquid sheet
Multiphase flow
VOF model

ABSTRACT

The present paper focuses on the mathematical modeling of industrial fan spray atomizers. The two-phase flow taking place inside the nozzle's tip and the exterior region near the outlet of three different industrial nozzle designs has been modeled and simulated. As a result, valuable information has been obtained regarding the influence of the inner geometry on the flow and also the formation and development of the liquid sheet. Characteristic magnitudes such as the discharge coefficient and the liquid sheet thickness factor have been obtained and validated through experimental measurements. The accumulation of liquid at the border of fan-shaped liquid sheets, also known as rim, has been studied in the analyzed designs, revealing the presence of a tangential velocity component in the liquid sheet and a relationship between the incoming flow rate of the rim and the angle of the liquid sheet. The dependence of the results on turbulence modeling has also been analyzed, drawing interesting conclusions regarding their influence on the liquid sheet mean flow characteristics and on the surrounding gas. Thus, the mathematical model developed has been proved to be a useful tool for nozzle manufacturers; it provides the most important characteristic parameters of the liquid sheet formed given certain nozzle geometry and, additionally, those data necessary to carry out studies of instability, breakup and atomization of the liquid sheet.



## 1. Introduction

The main objective of liquid atomization is to transform a bulk of liquid into drops in a gaseous atmosphere so that a maximum surface to volume ratio is achieved. It is employed in many industrial processes and practical applications including combustion, painting, spray cooling, agriculture and powder metallurgy, each having its own requirements on the spray features (Lefebvre, 1989). Knowledge of atomization processes and spray dynamics allows the adjustment to these particular requirements so that a more efficient use of the atomized fluid is achieved. As a consequence, since the first contributions of Rayleigh (1878) at the end of the 19th century, followed by other researchers like Weber (1931) or Ohnesorge (1936), sprays have been the object of intensive research. Thanks to this interest, outstanding improvements have been achieved, including experimental devices for spray characterization or the development of complex mathematical models. However, these advances in the understanding of atomization have also revealed the complexity of its nature and the subsequent difficulty in developing a mathematical model of the global process.

Broadly speaking, works dealing with the atomization process can be divided into two categories: one focused on the experimental study of the atomizers' behavior and the determination of the physical phenomena taking part in the development, destabilization and subsequent breakup of the liquid stream and droplet distortion and interaction; the other on the mathematical modeling of the physical processes observed.

Within the first group, initially, great interest was generated in fan-shaped or radially expanding liquid sheets as shown in the work of Dombrowski et al. (1960), Dombrowski and Hooper (1962) and Fraser et al. (1962), where the mechanisms of formation, destabilization and breakup of this kind of sheets were first described. They may be formed by impingement of two jets, obstruction of one jet or use of a fan spray nozzle; presenting several special features that increase the difficulty of their modeling, such as attenuating thickness or the accumulation of liquid at the edges of the sheet. More recently, the studies developed by Bremond and Villermaux (2006), Bush and Hasha (2004) on the liquid sheets formed by collision of two jets are remarkable. However, along the years this interest has lessened, shifting towards plane sheet, cone and jet atomizers. Additionally, although many experimental, analytical and numerical mathematical modeling techniques have been developed for spray characterization, the use of real atomizers has been left aside by more simple and ideal configurations, since their small size increases the difficulty of experimental measurements. Actually, on fan spray atomizers the literature is scarce, standing out the numerical simulation of the flow inside the tip of the atomizer carried out by Zhou et al. (1996) and the analysis of droplet-size distributions by Schegk et al. (1985).

* Corresponding author. Tel.: +34 943 219 877; fax: +34 943 311 442.
*E-mail address:* maltimira@tecnun.es (M. Altimira).

0142-727X/$ - see front matter © 2008 Elsevier Inc. All rights reserved.
doi:10.1016/j.ijheatfluidflow.2008.12.006

**Nomenclature**

| | |
|---|---|
| $A$ | nozzle outlet cross-section ($m^2$) |
| $C_D$ | discharge coefficient (−) |
| $h$ | half sheet thickness (m) |
| $k$ | turbulent kinetic energy ($m^2/s^2$) |
| $K$ | thickness factor ($m^2$) |
| $p, P, p'$ | pressure field, mean, fluctuation (Pa) |
| $q$ | flow rate ($m^3/s$) |
| $r$ | radial coordinate (m) |
| $r'$ | modified radial coordinate (m) |
| $u, U, u'$ | velocity field, mean, fluctuation (m/s) |
| $\alpha, \bar{\alpha}, \alpha'$ | liquid volume fraction field, mean, fluctuation (−) |
| $\Delta P$ | operating pressure (Pa) |
| $\varepsilon$ | turbulent dissipation rate ($m^2/s^3$) |
| $\kappa$ | curvature of the liquid sheet ($m^{-1}$) |
| $\varphi$ | angular coordinate (−) |
| $\mu$ | dynamic viscosity (kg/m s) |
| $\theta$ | liquid sheet angle (−) |
| $\rho$ | density ($kg/m^3$) |
| $\sigma$ | surface tension (N/m) |
| $\omega$ | specific dissipation rate ($s^{-1}$) |

*Subscripts*

| | |
|---|---|
| $o$ | nozzle outlet |
| $l$ | liquid phase |
| $g$ | gas phase |

Works from the second category began with those developed by Squire (1953), Hagerty and Shea (1955) where the temporal linear instability of plane inviscid liquid sheets was analyzed. Several contributions followed where effects like viscosity (Jeandel and Dumouchel, 1999), velocity profiles (Ibrahim, 1997) or non-linearity (Mehring and Sirignano, 1998) were added to the mathematical models of temporal and spatial growth of instabilities and subsequent breakup of the liquid stream. An extensive review of these papers can be found in Sirignano and Mehring (2000). Recently, some publications have tackled the numerical simulation of the primary atomization process, like those by Herrmann (2002), Klein (2005) or Menard et al. (2007). However, only a few tackle the effect of turbulence (Lakehal et al., 2002) and those in which the nozzle geometry is considered are limited to simple configurations.

The present paper is focused on the mathematical modeling of industrial fan spray atomizers. This kind of atomizers is mainly used in agricultural and painting applications, where the knowledge of the spatial distribution of droplets and their average size is of major importance: droplets which are too small can be drifted by the surrounding air and placed in undesirable locations (Smith and Miller, 1994), while too large droplets would lead to an excessive liquid consumption and a non-uniform distribution throughout the target. Final droplet sizes and their spatial distribution are determined by the flow taking place upstream of the breakup region and even upstream of the liquid sheet formation. Thus nozzle geometry plays a fundamental role in the atomization process and, therefore, will be considered in this study.

In this paper the suitability of CFD techniques in the characterization of industrial fan spray atomizers is shown. The flow taking place inside the nozzle's tip and the exterior region near the outlet of the atomizer has been modeled providing valuable information regarding the influence of the inner geometry on the flow and also on the formation and development of the liquid sheet. The calculation entails several difficulties, since it combines an internal single-phase flow with an external two-phase flow, featuring large pressure and velocity gradients. Interesting magnitudes such as the discharge coefficient and the liquid sheet thickness factor have been obtained, as well as other results about the spatial distribution of the fluid and the production of turbulence. It should be underlined that the objective of the mathematical model presented is not the prediction of the destabilization and breakup of the liquid sheet, but the assessment of a suitable and robust tool for nozzle design that, in addition, provides the necessary data for the study of instability, breakup and atomization of the liquid sheet.

## 2. Description of the studied atomizers

In the most common type of fan spray atomizers the liquid is discharged through an orifice whose shape is given by the intersection of a wedge with a hemispherical cavity. The liquid stream

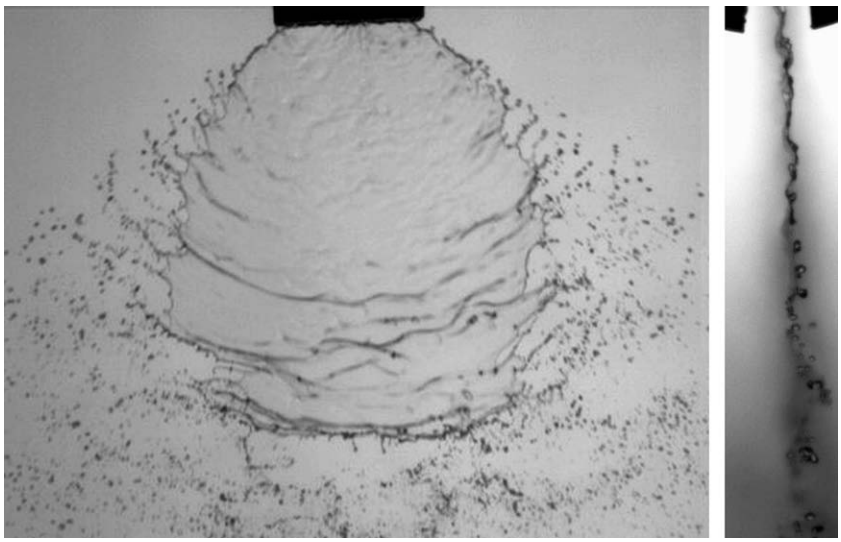

**Fig. 1.** Fan spray liquid sheet front view (left) and side view (right).

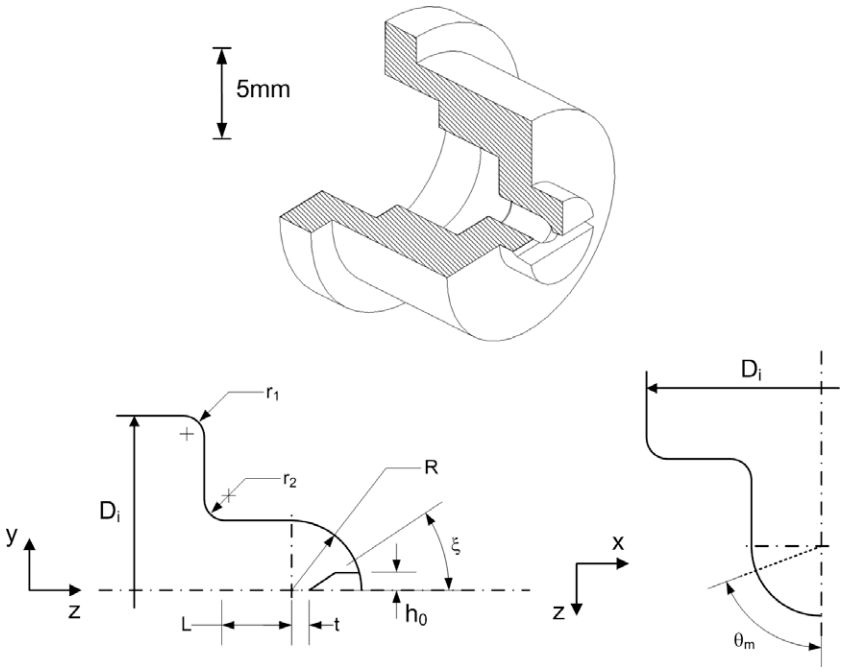


**Fig. 2.** Geometry of the atomizers.

formed is a fan-shaped sheet parallel to the major axis of the orifice, as can be seen in Fig. 1, where front and side views of the liquid sheet produced by one of the studied atomizers are presented.

In this work, three different industrial designs of fan spray atomizers, henceforth named $N_1$, $N_2$ and $N_3$, have been studied. These nozzles are usually employed in agricultural applications and were designed so that, under nominal operating conditions of 3 bar, they provide a flow rate of 0.8 l/min but different liquid sheet angle: $N_1$ provides a liquid sheet of 90°, $N_2$ of 80° and $N_3$ of 120°. All of them are tiny plastic units with circular section geometry ending in a hemispherical cavity. Despite their similar geometries, the three designs differ in their inner dimensions, as well as in the transition between different cross-sectional areas and in the shape of the outlet. The geometry of the designs is rendered in Fig. 2 while the main parameters defining their geometry are listed in Table 1.

Regarding the dimensions of the nozzles, it should be underlined that, due to the injection manufacturing process, there is an uncertainty in their values. Plastic injection pressure, mold temperature and nozzle cooling have a strong influence on the final dimensions and also on edge and surface finishing. Several units of each design were cut in half and measured by means of a CNC vision measuring system (Mitutoyo, QV PRO 302) to check the validity of the dimensions prior to their addition into the model. Images from cut units of the three designs are shown in Fig. 3.

Nozzle $N_1$ provides an even flat fan spray thanks to its orifice shape, whose wedge cut height ($h_0$) is limited. Its cross-sectional area reductions are round-edged and represented by radii $r_1$ and $r_2$ (Fig. 2). CNC measurements detected significant variations in the inner dimensions of several units of this design, as well as an unwanted round edge at the orifice, which is clearly distinguished in Fig. 3 (left). These features were added to the geometry of the model and, as will be demonstrated below, turned out to influence nozzle performance.

On the other hand, $N_2$ and $N_3$ provide a flat fan spray through an elliptically-shaped orifice, its wedge cut determined only by the $\xi$ angle value and feature sharp-edged cross-section reductions. CNC measurements revealed a close accordance between real and plan dimensions and, as can be seen in Fig. 3 (center and right), the absence of any appreciable round edge at the orifice for both designs.

**Table 1**
Geometrical parameters of the atomizers.

| Global parameters | | Outlet parameters | |
|---|---|---|---|
| $D_i$ | Inlet diameter | $t$ | Cut offset |
| $R$ | Tip radius | $\theta_m$ | Maximum outlet angle in sheet plane |
| $L$ | Tip length | $h_0$ | Wedge cut height limit |
| $r_1$, $r_2$ | Round radii | $\xi$ | wedge angle |

## 3. Mathematical model

### 3.1. Flow domain

The considered domain includes the tip of the nozzle and the exterior region near the orifice, as depicted in Fig. 4. According to the results obtained by Zhou et al. (1996), only the tip was modeled out of the whole inner geometry, since it is in this region where the most critical features of the flow are developed. Additional information about the domain selection can be found in Rivas et al. (2005).

The dimensions of the exterior zone are a critical issue in this study and are determined by the following criteria. Firstly, as the main objective of this work is the study of the liquid sheet development, but not the appearance or growth of instabilities leading to its breakup, the length ($Z$ direction) of the domain was chosen sufficiently short (between 3% and 9% of the breakup length) to ensure small amplitude of the perturbations, in case they exist. Secondly, the attenuating thickness of the liquid sheet has also been taken into account, since the longer the domain the higher the number of elements necessary to guarantee a good resolution inside the sheet, involving higher computational cost. However, this fact was less restrictive than the amplitude of the instabilities. The dimension perpendicular to the liquid sheet ($Y$ direction) is such that the boundary condition is not affected by the shear layer

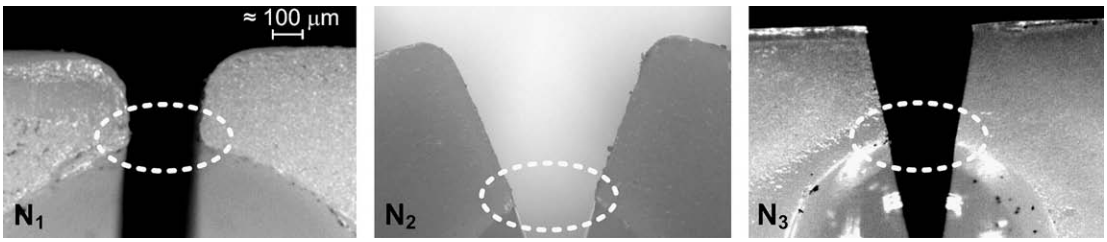


**Fig. 3.** Image from $N_1$ (left), $N_2$ (center) and $N_3$ (right) cut units.

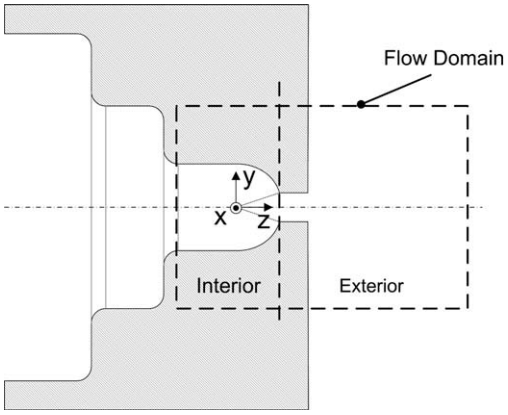


**Fig. 4.** Flow domain.

formed at the vicinity of the liquid sheet. Finally, the minimum width of the domain ($X$ direction) was fixed by its length and the angle of the liquid sheet.

The geometry of the nozzles allows the simplification of the domain using two symmetry planes ($XZ$ and $YZ$). Since the length of the domain is such that the perturbations have very small amplitude and a stationary solution is wanted, it is reasonable to assume also the symmetry of the mean flow. Thus only a quarter of each geometry has been modeled.

### 3.2. Governing equations

The two fluids of interest, i.e. water and air, have been considered incompressible, being their ratios of density ($\rho_g/\rho_l$) and dynamic viscosity ($\mu_g/\mu_l$) 0.00123 and 0.0178, respectively. Posing the multiphase flow problem, the conservation equations for mass and momentum should be fulfilled for each phase separately,

$$\frac{\partial u_{i,k}}{\partial x_i} = 0 \tag{1}$$

$$\frac{\partial}{\partial t}(\rho_k u_{i,k}) + \frac{\partial}{\partial x_j}(\rho_k u_{i,k} u_{j,k}) = -\frac{\partial p_k}{\partial x_i} + \frac{\partial}{\partial x_j}\left[\mu_k \cdot \left(\frac{\partial u_{i,k}}{\partial x_j}\right)\right] \tag{2}$$

where $k = g$ for the gas phase and $k = l$ for the liquid phase. At the interface, the following kinematic and dynamic boundary conditions should be imposed:

$$\begin{aligned} &[u_i] = 0 \\ &[(\tau_{ij} \cdot n_i) \cdot n_j + p] = \sigma \cdot \kappa \\ &[(\tau_{ij} \cdot n_i) \cdot t_j] = 0 \end{aligned} \tag{3}$$

being

$$[\,] = (\,)_l - (\,)_g \tag{4}$$

$n_i$ and $t_j$ the $i$th and $j$th components of the vector normal (from liquid to gas phase) and tangent to the interface, respectively, and $\kappa$ the curvature of the interface.

In multiphase and multifluid flows described by Eqs. (1)–(4), the position, shape, dynamics and all the phenomena associated to the interface are of great interest. Several methods (Lakehal et al., 2002) have been and are still being proposed to simulate these flows, which can be classified in two approaches according to the way they consider the flow domain and its discretization.

The first approach includes those methods where each phase or fluid features a deformable flow domain which must be discretized to solve Eqs. (1)–(4) at each time step (Ryskin and Leal, 1984). In these methods, the definition of the interface geometry and jump conditions is straightforward, since the interface is simply the boundary between different domains. However, difficulties arise in these models when dealing with high distorted domains.

The second approach considers a unique flow domain, which is usually fixed; and the geometry, position and time evolution of the interface have to be determined through an additional procedure. Consequently, in this approach there exists only one system of differential equations for one fluid (mixture). Different phases or fluids are modeled allowing spatial variation of fluid properties (density and viscosity) and jump conditions are modeled including source terms in the flow equations. This approach can be, in turn, divided into two categories according to the method employed to identify the interface. The first one includes those known as front-tracking methods, where particles (Lagrangian markers) are used to identify the interface (Harlow and Welch, 1965). Methods from the other category are called front-capturing, since they use a mark function (also called scalar or color function) to locate the interface, this function being solved with an additional differential equation. Volume of Fluid (VOF) (Hirt and Nichols, 1981; Nardone et al., 1994) and Level Set (Zhu and Sethian, 1992) are well known front-capturing methods and several modifications (Gueyffier et al., 1999) and combinations of both methods have been proposed to improve their performance (Sussman et al., 2007).

In this work, the VOF method has been used, since it features a conservative formulation and allows for the direct finding of a steady solution (if this exists) of the flow. In this method, the volume fraction ($\alpha$) of the secondary phase (liquid) is used as marker function and the following transport equation is used:

$$\frac{\partial \alpha}{\partial t} + \frac{\partial}{\partial x_i}(\alpha u_i) = 0 \tag{5}$$

As a function of the local value of liquid volume fraction, values of properties like density and viscosity are evaluated with the following averaging:

$$\begin{aligned} \rho &= \alpha\rho_l + (1-\alpha)\rho_g \\ \mu &= \alpha\mu_l + (1-\alpha)\mu_g \end{aligned} \tag{6}$$

And the governing equations result

$$\frac{\partial \rho}{\partial t} + \frac{\partial \rho u_i}{\partial x_i} = 0 \tag{7}$$

$$\frac{\partial}{\partial t}(\rho u_i) + \frac{\partial}{\partial x_j}(\rho u_i u_j) = -\frac{\partial p}{\partial x_i} + \frac{\partial}{\partial x_j}\left[\mu \cdot \left(\frac{\partial u_i}{\partial x_j}\right)\right] + (F_V)_i \tag{8}$$

$$(F_V)_i = \sigma \cdot \kappa \cdot n_i \cdot \delta$$

Since both phases share the same velocity field, the interface kinematic boundary condition is automatically fulfilled. The normal stress jump condition given by surface tension is introduced

into the momentum equation as a source term through a Dirac's delta function, which has been modeled through the Continuum Surface Force (CSF) model (Brackbill et al., 1992) (Eq. (9)). This model interprets surface tension as a three-dimensional continuous effect across the interface rather than as a boundary condition. A volume force equivalent to the surface tension force is derived in terms of a variable which presents a discontinuity at the interface such as density, and introduced at the momentum equation. Gravitational force should also be added as another source term in Eq. (8). Nevertheless, values of the Froude number in the range of operating pressures considered indicate that its effects can be neglected without detriment to the description of the phenomena.

$$(F_V)_i = \sigma \cdot \kappa \cdot \frac{\frac{\partial \alpha}{\partial x_i} \cdot \rho}{\frac{1}{2}(\rho_g + \rho_l)} \tag{9}$$

Recently, several works (Yeh, 2005; Rivas et al., 2005; Liovic and Lakehal, 2006) have underlined the importance of turbulence in nozzle performance, turning its modeling into a major issue. However, the number of studies dealing with turbulence effects on the interface is small, and almost null with RANS approach. With the aim of determining the influence of turbulence modeling for the present case, the flow has been simulated using different turbulence models, namely: k-ε Standard, RNG and Realizable and k-ω SST. Since the flow is turbulent within the domain, magnitudes can be divided into mean and fluctuating components.

$$\begin{aligned} \alpha &= \bar{\alpha} + \alpha' \\ u_i &= U_i + u_i' \\ p &= P + p' \end{aligned} \tag{10}$$

Performing Reynolds averaging following Shirani et al. (2006), the flow governing equations result in

$$\frac{\partial \bar{\rho}}{\partial t} + \frac{\partial \bar{\rho} U_i}{\partial x_i} = 0 \tag{11}$$

$$\frac{\partial \bar{\alpha}}{\partial t} + \frac{\partial}{\partial x_i}(\bar{\alpha} U_i + \overline{\alpha' u_i'}) = 0 \tag{12}$$

$$\frac{\partial}{\partial t}(\bar{\rho} U_i) + \frac{\partial}{\partial x_j}(\bar{\rho} U_i U_j + \bar{\rho}\overline{u_i' u_j'}) = -\frac{\partial P}{\partial x_i} + \frac{\partial}{\partial x_j}\left[\overline{\mu} \cdot \left(\frac{\partial U_i}{\partial x_j}\right)\right] + (\overline{F_V})_i \tag{13}$$

where the overlined magnitudes stand for ensemble averaged values and

$$\begin{aligned} \bar{\rho} &= \bar{\alpha} \cdot \rho_g + (1 - \bar{\alpha})\rho_l \\ \bar{\mu} &= \bar{\alpha} \cdot \mu_g + (1 - \bar{\alpha})\mu_l \end{aligned} \tag{14}$$

After the averaging the following new terms have appeared and need to be modeled: $\overline{u_i' u_j'}$, $\overline{\alpha' u_i'}$ and $(\overline{F_V})_i$. The first term, $\overline{u_i' u_j'}$ (Reynolds stress term), has been modeled adopting the Boussinesq hypothesis. The second, $\overline{\alpha' u_i'}$, which represents the correlation between the fluctuations of volume fraction and velocity, would provide valuable information about the influence of turbulent scales on the liquid sheet dynamics. A modeling proposal for this term can be found in Shirani et al. (2006). From the results presented in that paper one can conclude that, in the region near the outlet of the atomizer, where turbulent disturbances present small amplitudes, the effects of this term on the mean flow magnitudes are not appreciable. Consequently, it has been omitted in the mathematical model. Finally, the last term corresponding to the fluctuations on the equivalent surface tension force has been calculated directly with the mean values of the variables.

A discussion between the turbulence models employed is developed in a further section, where the distribution of turbulent quantities within the domain and also their influence on the most important characteristic parameters of the flow will be appraised. At this point it should be reminded that, since a one-fluid formulation is used, both phases share the same fields for turbulent magnitudes and that no special treatment has been imposed on the interface.

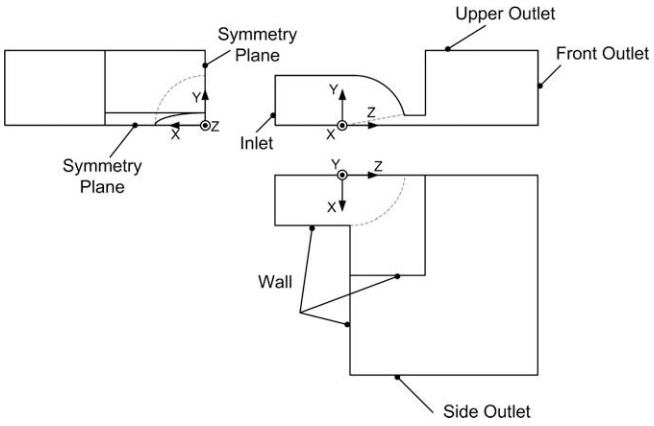


**Fig. 5.** Boundary conditions.

The Standard k-ε model (Launder and Spalding, 1972) has been for many years the most commonly used turbulence model, due to its simplicity and robustness. Knowledge of its strengths and weaknesses has favored the development of more complete k-ε based models, such as the RNG (Yakhot and Orszag, 1986), which is derived from the instantaneous Navier–Stokes equations by means of Renormalization Group Methods, or the Realizable (Shih et al., 1995). Regarding near-wall effects, they are significant only inside the nozzle and the external region near the orifice, where the meshes employed guarantee a proper resolution of the viscous sublayer throughout the wall boundaries in all the conditions under study. In simulations with k-ε turbulence modeling, the two-layer model of Chen and Patel (1988) has been combined with enhanced wall functions using the blending functions proposed by Kader (1981).

The k-ω SST model (Menter et al., 2003), which combines the Standard k-ω formulation in the near-wall region and a transformed k-ε model in the far field, has also been employed in the simulations. Because of its approach, the model is valid throughout the near-wall zone as long as there is a good mesh resolution, and therefore no special near-wall modeling is required.

### 3.3. Boundary conditions

Boundary conditions for the liquid and gas flow are depicted in Fig. 5. At the tip inlet, profiles of total pressure, turbulent quantities as well as the velocity direction were enforced. All these data were obtained in previous simulations described in Rivas et al. (2005). At the walls, a non-slip condition was imposed, while at both symmetry planes the normal velocity component and the normal gradients of all other variables were set to zero. Finally, a zero-valued gauge pressure field was set at the three atmosphere boundaries with very small constant values of backflow turbulent intensity ($I = 4$) and viscosity ratio ($\mu_T/\mu = 10$) to represent a turbulence-free condition.

## 4. Simulation of the mathematical model

The commercial CFD code Fluent V.6.3 has been used to solve the mathematical model. In this code, the values for all fields are stored at the center of each cell. Therefore, for the calculation of convective and diffusive terms, the values at the cell faces must be interpolated from the surrounding cells. With this aim, a second order centered scheme has been chosen for diffusive terms whilst second order upwind (Barth and Jespersen, 1989) for convective terms at the continuity and momentum equations. The SIMPLE

algorithm (Patankar and Spalding, 1972) has been used to tackle pressure–velocity coupling, whereas for pressure interpolation, a staggered-grid based scheme has been used (Patankar, 1980).

The accuracy of the VOF model is strongly determined by the sharpness of the interface, since properties of the fluids and interfacial forces are replaced by smoothly varying values. So it is of crucial importance to avoid the smearing of the interface by means of an appropriate numerical differencing scheme for face flux calculation. In this aspect, neither upwind nor central differencing schemes are suitable, due to their diffusive nature. The use of special interpolating schemes such as Geometric Reconstruction (Youngs, 1982) or Donor–Acceptor (Hirt and Nichols, 1981) at the interface cells may provide an unsteady and more accurate representation of the interface, but at the expense of stability loss and increase in computational needs. Nevertheless, as previously mentioned, the length of the domain was chosen so that the amplitude of instabilities on the liquid sheet surface could be taken as negligible and a steady state solution could be attained. For this case, the combination of an implicit interpolation method with a modified High Resolution Interface Capturing (HRIC) scheme (Muzaferija and Peric, 1998) for face flux calculation provides an interface sharpness comparable to that obtained with Geometric Reconstruction, proper calculation stability and is less computationally expensive.

The HRIC scheme consists of a non-linear blending of Bounded Downwind (*BD*) and Ultimate Quickest (*UQ*) (Leonard, 1991) upwind differencing schemes, in such a way that the compressive property of the former and the stability of the latter are combined. A normalized cell volume fraction $\tilde{\alpha}_c$ is computed using the values of the upstream ($U$) and downstream ($D$) cells.

$$\tilde{\alpha}_c = \frac{\alpha_c - \alpha_U}{\alpha_D - \alpha_U} \tag{15}$$

Then, both *BD* and *UQ* schemes are used to calculate the normalized face volume fraction

$$(\tilde{\alpha}_f)_{BD} = \begin{cases} \tilde{\alpha}_c & \tilde{\alpha}_c < 0 \text{ or } \tilde{\alpha}_c > 1 \\ 2\tilde{\alpha}_c & 0 \leqslant \tilde{\alpha}_c \leqslant 0.5 \\ 1 & 0.5 \leqslant \tilde{\alpha}_c \leqslant 1 \end{cases} \tag{16}$$

$$(\tilde{\alpha}_f)_{UQ} = \begin{cases} \tilde{\alpha}_c & \tilde{\alpha}_c < 0 \text{ or } \tilde{\alpha}_c > 1 \\ MIN\left[(\tilde{\alpha}_f)_{BD}, \frac{6\tilde{\alpha}_c+3}{8}\right] & 0 \leqslant \tilde{\alpha}_c \leqslant 1 \end{cases} \tag{17}$$

and finally, both values are blended with a function of the angle formed between the normal to the interface and the normal to the cell face ($\zeta$).

$$\tilde{\alpha}_f = (\tilde{\alpha}_f)_{BD}\sqrt{cos\,\zeta} + (1 - \sqrt{cos\,\zeta})(\tilde{\alpha}_f)_{UQ} \tag{18}$$

The results obtained using this scheme have been compared with those provided by a second order upwind scheme, proving that the former is capable of reproducing a sharper interface.

The flow domain has been discretized with a 3 million element hybrid mesh. Although most of the elements are hexahedral, the sharp wedge cut at the orifice has been meshed with triangular prisms due to its complexity.

All numerical simulations have been carried out in an HP server Proliant DL585 with four dual core processors and 16 Gbyte RAM working at 2.4 GHz. The convergence criterion has been such that the scaled residuals from all the variables had to be below $10^{-6}$, entailing calculation time requirements between 100 and 180 h depending on the mesh density employed.

## 5. Verification of the mathematical model

For the verification of the mathematical model, an estimation of the discretization error, as well as a discussion about VOF differencing schemes have been carried out for design $N_1$. Due to the resemblance between the geometries and meshes of all three designs, studies for $N_2$ and $N_3$ have been considered unnecessary.

It should be underlined that, out of the discussion on turbulence modeling, only those results obtained with the k-ε RNG model will be presented from this point onwards since, as it will be seen, all turbulence models provide similar values for the liquid sheet mean flow variables.

In order to quantify the discretization error, calculations were carried out using a coarser and a finer mesh, applying a sizing factor ($s$) of 1.25 to the original solution. Hence, the coarse mesh consists of 1.5 million elements whilst the fine mesh has 6 million elements.

At first, the estimation was made by means of the Richardson extrapolation method (Richardson, 1927), using different characteristic quantities such as the liquid sheet thickness factor or the discharge coefficient. Although the chosen variables had extremely similar values for the original and the fine mesh, illogical values of the apparent order about six appeared, which may indicate that the coarse mesh was outside the asymptotical range of the discretization error. Consequently, the expression proposed by Roache (1998) for the Grid Convergence Index (GCI) calculation was adopted, assuming a conservative value for the safety factor of 3. Since only the original and the fine mesh are object of this convergence study, the apparent order ($g$) was taken as equal to the formal order of the scheme used, i.e. 2. Values for the fine mesh index of 2.3% and 3.8% were obtained for the thickness factor and the discharge coefficient, respectively.

Therefore, from the numerical accuracy point of view, the fine mesh should be used. However, computational needs for simulations with this mesh exceed the capacity of usually available computers. Since one of the purposes of this work is to provide an attainable tool oriented towards nozzle design, the use of this mesh was ruled out. From the GCI calculated for the fine mesh, the index corresponding to the original solution has been evaluated with the following expression (Roache, 1994), obtaining values of the GCI of 3.7% and 6% for both quantities.

$$GCI_{\text{original}} = s^g \cdot GCI_{\text{fine}} \tag{19}$$

Nevertheless, an analogous estimation of the discretization error undertaken with geometry $N_1$ excluding the round edge of the orifice gave a GCI for the original mesh under 2% for both the thickness factor and the discharge coefficient. Therefore, it can be concluded that the evaluation of the GCI is highly influenced by an extremely small parameter, i.e. the round edge radius, which is, at the same time, very difficult to take into account in the discrete mathematical model.

Following this, subsequent calculations including the discussions about discretization schemes and turbulence models have been run using the intermediate mesh.

When it comes to the interface sharpness, simulations have been carried out using two different differencing schemes, namely HRIC and second order upwind, for the VOF equation. Contours of liquid volume fraction at surfaces with maximum radial coordinate are represented in Fig. 6 for both schemes. These surfaces feature the thinnest liquid sheet and the largest volume fraction diffusion, making even more evident the superiority of the HRIC scheme in the resolution of the boundary.

The choice of the spatial discretization scheme has turned out to have more influence on the border of the liquid sheet than on the sheet itself. Hence, results for the flow rate, the discharge coefficient or the mean thickness factor are not significantly affected. However, due to numerical diffusion and the adopted definition of the interface, the calculation corresponding to the second order upwind scheme exhibits a smaller rim and, consequently, a lower liquid sheet angle.

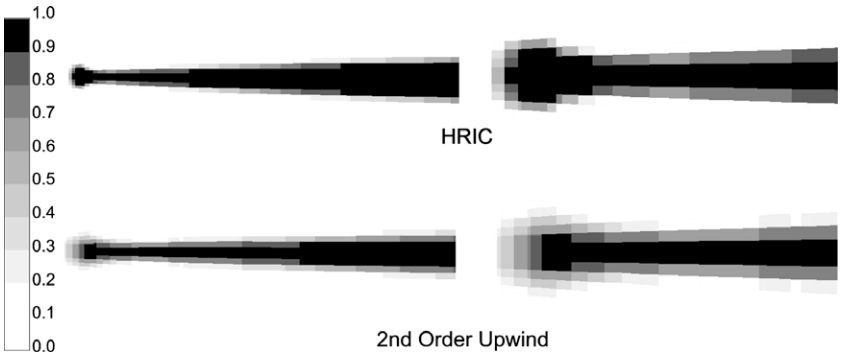


**Fig. 6.** Contours of liquid volume fraction. HRIC vs. second order upwind scheme.

## 6. Validation of the mathematical model

Experimental validation has been carried out by assessing the prediction of the mathematical model for several measured flow features. All the measurements have been carried out in different units of every considered design, in order to minimize the effect of manufacturing irregularities.

VOF based calculations do not provide a clear and sharp interface between the fluids but a continuous profile of volume fraction. The interface is then identified by the presence of few adjacent cells with $\alpha$ values between 0 and 1. So, prior to extracting any result it has been necessary to define a criterion for the definition of the interface, taken as the isosurface with 0.5 liquid volume fraction (Lafaurie et al., 1993).

Additionally, for the sake of a clear representation of the results, a cylindrical coordinate frame has been set (Fig. 7). The origin is fixed at the intersection between symmetry planes and the line tangent to the liquid sheet. This point was defined by Dombrowski et al. (1960) as the pressure center of the liquid sheet. The modified radial coordinate $r'$ has been established as the radial coordinate minus the tip radius. Dimensionless magnitudes have been defined taking $A^{1/2}$ and $(2\Delta P/\rho_l)^{1/2}$ as the characteristic length and velocity, respectively. These characteristic magnitudes, together with the properties of the liquid phase, have been used to calculate the Reynolds number of the liquid sheet.

### 6.1. Liquid sheet angle

Liquid sheet angle ($\theta$) is one of the most important characteristic parameters of fan spray atomizers, since it is directly related to the coverage of the spray. Experimental angles were measured at 25 images randomly selected from a set of 500 frames captured with a Redlake MotionXtra HG100-LE high speed camera along the whole pressure range. Table 2 shows the comparison of the measured mean values, together with the 95% confidence interval, and predicted values of $\theta$. Results from $N_1$ and $N_3$ show good agreement, with errors lower than 8%; whereas those from $N_2$ present errors up to 18%.

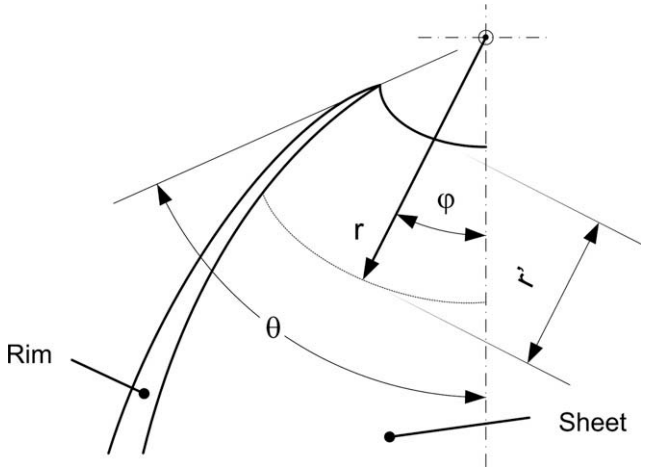


**Fig. 7.** Reference frame and magnitudes.

### 6.2. Discharge coefficient

Another major performance parameter is the discharge coefficient $C_D$, defined as

$$C_D = \frac{q_l}{A \cdot \left(\frac{2\Delta P}{\rho_l}\right)^{1/2}} \tag{20}$$

For the experimental measurement of the discharge coefficient a pressure transmitter (Wika S10) and an ultra-low flow sensor (Omega FTB-601) were used. In order to minimize the influence of the flow sensor operation curve on the measurements, it was previously calibrated with the stream gauging method determining the constant of proportionality between pulses and liquid volume for the whole range of operating pressures. An error in $C_D$ measurements of ±3% has been estimated considering the flow meter, pressure transmitter and data acquisition frequency as the major error sources.

**Table 2**
Variation of liquid sheet angle (°) with pressure. Predicted vs. measured values with 95% confidence interval.

| $P$ (bar) | $N_1$ | | $N_2$ | | $N_3$ | |
|---|---|---|---|---|---|---|
| | Predicted | Measured | Predicted | Measured | Predicted | Measured |
| 1 | 42.8 | 40.6 ± 0.6 | 37.0 | 36.8 ± 1.8 | 53.3 | 55.2 ± 3.1 |
| 2 | 44.0 | 43.0 ± 0.3 | 44.6 | 37.8 ± 1.2 | 55.0 | 58.0 ± 1.4 |
| 3 | 44.0 | 44.0 ± 0.4 | 45.5 | 39.6 ± 1.0 | 56.6 | 60.4 ± 1.2 |
| 4 | 44.1 | 46.3 ± 0.6 | 45.9 | 41.4 ± 0.9 | 57.0 | 61.6 ± 0.8 |

Fig. 8 depicts the variation with pressure of this parameter for $N_1$ and $N_2$. It is noticeable that small variations in the inner dimensions of $N_1$ units due to the manufacturing process lead to a higher scattering of the experimental data. Additionally, results from $N_1$ prove the importance of considering the round edge, since its addition to the geometry improves significantly the prediction of the discharge coefficient, decreasing the average error from 25 to 8%. In nozzles of design $N_2$, by opposite, real dimensions presented good agreement with design dimensions and a very accurate prediction of $C_D$ was obtained for this design, with 5% error along the studied range of operating conditions. Finally, values for the discharge coefficient from simulations of $N_3$ present errors between 7% and 15% at the range of 1–4 bar and 20% at 0.5 bar.

### 6.3. Thickness factor

This parameter ($K$) was first defined by Dombrowski et al. (1960) and Taylor (1960) as the ratio between the liquid sheet half thickness ($h$) at any point and its radial coordinate ($r$). It is an essential parameter in the stability analysis of an attenuating liquid sheet, an issue tackled by authors like Weihs (1978) and Clanet and Villermaux (2002).

$$h = \frac{K}{2r} \tag{21}$$

Dombrowski et al. (1960) stated that $K$ was constant from a certain operating pressure on. Based on that statement, in several papers (Dombrowski and Hooper, 1962; Weihs, 1978) it was assumed to be a constant characteristic parameter. Values of this parameter along the sheet obtained from simulations of the mathematical model have been plotted at different dimensionless radial coordinates and are shown in Fig. 9.

It can be seen that the thickness factor of the liquid sheet varies both with the radial and the angular coordinate, the former being strongly related to the shape of the orifice, which has also been depicted at the lower left corner of each chart. For the sake of clarity, profiles at only two dimensionless radial coordinates have been depicted. However, it should be pointed out that, in the presented simulations, further downstream this factor tends to a value independent of the radial coordinate. The growth of the rim while moving downstream is clearly represented, and will be analyzed in a following section.

Observing the profiles from $N_1$ with and without the round edge (left and centered charts); one can conclude that the presence of this feature changes completely the appearance of the liquid sheet, its thickness factor and the development with the radial coordinate.

Despite the observed variations of this parameter with the position inside the liquid sheet, and with a view to the development of a subsequent model dealing with the instability of an attenuating liquid sheet, it is advisable to get an averaged value of $K$ from CFD calculations. This value has been calculated using an area-weighted averaging throughout the liquid sheet excluding its border and the region where the flow is highly influenced by the orifice, and is depicted in Fig. 10 for the three studied designs along the range of operating pressures. The lack of dependence of the averaged thickness factor with the operating pressure is noticeable; one may thus conclude that this magnitude can be defined as a characteristic parameter of a nozzle.

An interferometric technique proposed by Dombrowski et al. (1960) and lately used by other authors (Choo and Kang, 2001; Clanet and Villermaux, 2002; Lan et al., 2008) has been used to measure the sheet thickness variation experimentally. It consists of illuminating the liquid sheet with a monochromatic light beam. Due to the attenuating thickness, reflections from the front and the back surfaces of the sheet present different optical paths and create a pattern of constructive and destructive interference. This phenomenon is represented schematically in Fig. 11.

The optical path difference $\Theta$ for a liquid sheet of half thickness $h$ can be expressed as

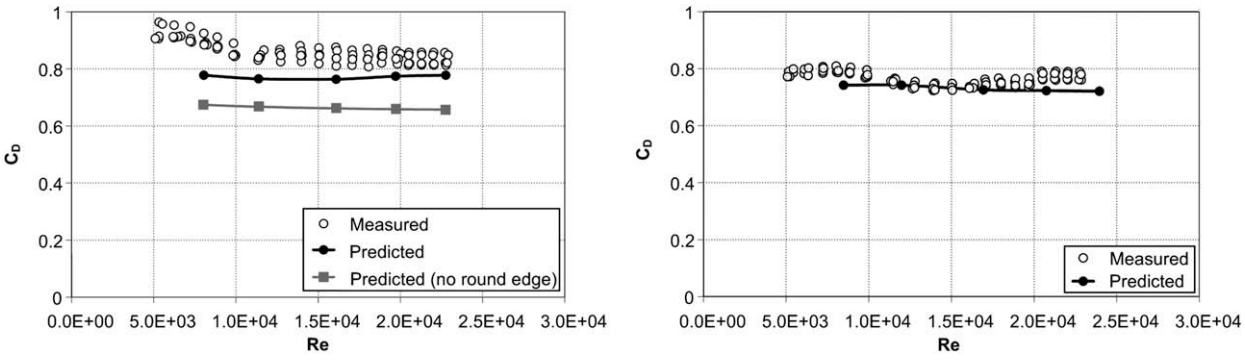


**Fig. 8.** Measured vs. predicted values of the discharge coefficient for $N_1$ (left) and $N_2$ (right).

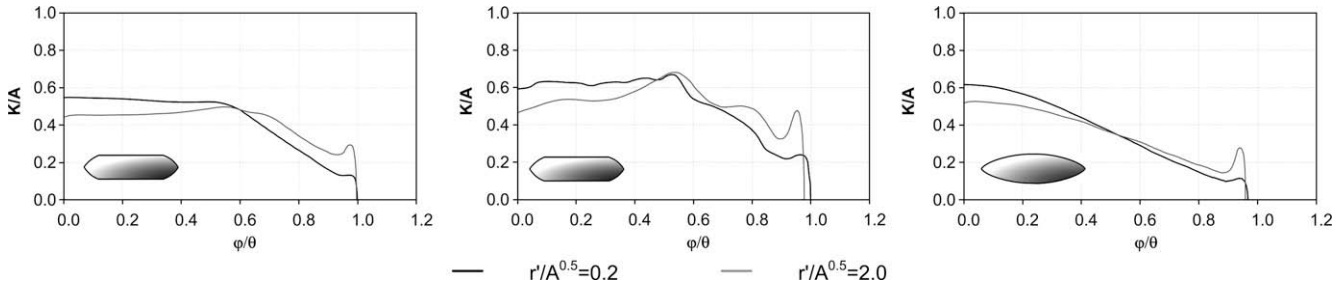


**Fig. 9.** Angular profile of dimensionless thickness factor $K$ at different dimensionless radial coordinates for $N_1$ without round edge (left), with round edge (center) and $N_3$ (right) at 3 bar.

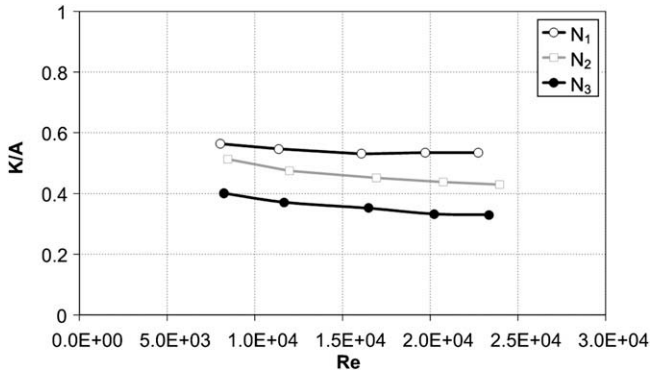


**Fig. 10.** Variation of the dimensionless thickness factor $K$ with operating conditions for $N_1$, $N_2$ and $N_3$.

$$\Theta = \eta(\overline{AB} + \overline{BC}) - \overline{AD} = 2\eta \cdot 2h \cdot \cos\beta \tag{22}$$

$\eta$ and $\beta$ being the refractive index and the refraction angle of the light on the liquid sheet, respectively. Where $\Theta$ is an odd number of times the half-wavelength of the incident light, a bright fringe appears. Therefore, the thickness variation between two adjacent bright fringes can be written as

$$\Delta h = \frac{\lambda}{4\eta\cos\beta} \tag{23}$$

The relation between the incident and refraction angles is given by $\sin\beta = \eta\sin\phi$. Thus the thickness factor can be expressed as

$$K = \frac{\lambda}{\eta\left(1 - \frac{\sin^2\phi}{\eta^2}\right)^{1/2}} \cdot \frac{q - t}{\frac{1}{r_t} - \frac{1}{r_q}} \tag{24}$$

$r_q$ and $r_t$ being the radial coordinates for the $q$th and the $t$th fringes, respectively.

The light source used was a 1000 W mercury vapor lamp with a discrete spectrum of emission. A plano-convex lens and a band-pass filter were placed in front of the lamp to produce a parallel light beam of a single wavelength. A CCD camera (Nikon D80) with a macro lens was used to capture the images.

As the calculated thickness factor depends on $\sin\phi$, taking a smaller value for $\phi$ minimizes the error determining $\phi$. So the optical arrangement was lined up and placed in front of the liquid sheet with a 10° slant from its normal and the camera was placed symmetrically, so most of the reflected light was received by the CCD sensor.

An estimation of the experimental error has been carried out, establishing $\phi$, $r_q$ and $r_t$ as the major error sources. The angle between the incident light and the camera and the normal to the liquid sheet ($\phi$) is controlled by means of two rotary plates with a precision of ±1°. On its turn, $r_q$ and $r_t$ introduce an error related to the width of the fringes. Considering the typical values of these parameters in the most unfavorable combination, an error of 6% in thickness factor measurements has been estimated.

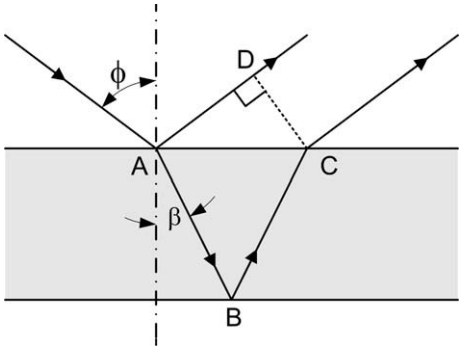


**Fig. 11.** Optical paths of the interference phenomenon.

Nevertheless, this technique is extremely sensitive to the presence of perturbations, as previously noticed by Fraser et al. (1962). The appearance of random disturbances on the sheet's surface makes impossible the formation of the interference pattern, as shown in Fig. 12. The visualization of fringes near the outlet, where the amplitude of perturbations is smaller, was also impossible since, due to the fast thickness reduction, the fringe spacing is extremely short. At very low operating pressures, the formation of perturbations causes difficulties for measurements at sufficiently distant and unperturbed points. So, finally, measurements were achievable only in units of $N_1$ at operating pressures between 1 and 3 bar.

As previously seen, the value of the thickness factor varies with the angular coordinate due to the orifice shape. Thus, this parameter was measured at different angular positions $\varphi$ between −20° and 20°.

Discrete values of $K$ obtained in measurements of $N_1$ are depicted in Fig. 13, revealing the presence of high data dispersion in measurements at different positions. However, as already stated for the mean values throughout the liquid sheet from CFD simulations, there is no relevant dependence on the operating pressure. This confirms that $K$ can be defined as a characteristic parameter of each nozzle design. In Fig. 13 are also presented the range of values of the thickness factor obtained from simulations at the region of the liquid sheet equivalent to the measurement position range, i.e. at angular positions between −20° and 20°.

### 6.4. Spatial distribution of the spray

The spatial distribution of the spray produced was measured experimentally with a Patternator, a device consisting of a set of test tubes uniformly distributed at a certain vertical distance from the nozzle (Fig. 14). It should be pointed out that these measurements are very common amongst nozzle manufacturers. Obviously, the final distribution of the spray is highly influenced by the atomization process, whose modeling is not inside the scope of this work, but it is possible to get a reliable flow distribution with the data from the simulations, contributing to the validation of the mathematical model and providing a useful tool with a view to nozzle design.

To obtain the desired data from the simulations, the front outlet boundary (Fig. 5) of the considered domain was divided into regions with surface equivalent to a patternation test tube. The mass flow rate passing through each region was computed and related to the global mass flow rate providing values easily comparable with the experimental results.

In Fig. 15, the right chart corresponds to the flow distribution of $N_3$, the level of agreement being noteworthy between the mathematical model and the experimental values for this case, where only at the border of the spray small differences can be observed. These are due to the highly disturbed real sheet, which provokes its prompt destabilization preventing the formation and growth of the rim. Adjustment of the results from $N_2$ is similar to that from $N_3$, since both liquid sheets present the same behavior. However, the prediction of flow rate distribution at the center of the liquid sheet is not as accurate. Finally, results for $N_1$ at 3 bar present a considerable lack of fit at the border, since the liquid leaves the nozzle completely undisturbed and the rim is formed and grows as it travels downstream.

So the prediction of angular flow rate distribution given by simulations is very accurate in those cases where the liquid sheet perturbations prevent the formation of the rim. Considering a more

**Fig. 12.** Images captured with the interferometric technique. (Left) 0.5 bar, (center) 1.5 bar, (right) 3 bar.

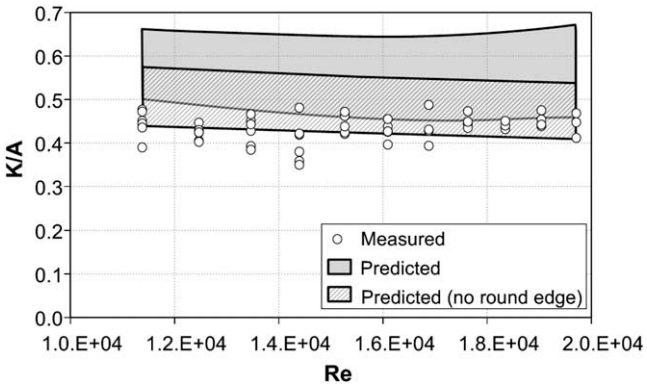


**Fig. 13.** Measured vs. predicted values of the thickness factor for $N_1$.

**Fig. 14.** Experimental device employed for flow distribution measurements (Patternator).

extensive domain may improve the results in small disturbance cases, but at the expense of modeling a region with larger perturbations whose dynamics cannot be predicted with the model used.

## 7. Results and discussion

In addition to the outcomes presented throughout the validation of the mathematical model, other relevant results have been obtained through the analysis of data from CFD simulations. Along the following lines discussions regarding the velocity profile of the liquid sheet or the growth of the rim will be developed, giving special attention to the differences on the behavior of the nozzles under study and their underlying grounds.

One of the main drawbacks of fan spray atomizers is the accumulation of liquid at the free edge of the sheet, forming the so called rim. The breakup of the rim follows the mechanism of a free jet, producing larger droplets than the ones from the liquid sheet and leading to disturbed flow (Fig. 15; left) and droplet-size distributions (Fig. 16a). Depending on the flow regime, it can even influence the destabilization of the liquid sheet enhancing its breakup (Sirignano and Mehring, 2000).

In order to make a separate analysis, the region of the liquid sheet corresponding to the rim has been differentiated from the liquid sheet itself in the different calculations. Then, from this point onwards presented results will refer to the liquid sheet and the rim separately.

From the results detailed in Table 3 one can notice that, in agreement with experimental visualizations (Fig. 16), the rim enlarges with the distance from the orifice, the one produced by $N_1$ being larger than the one by $N_3$. At higher operating pressures the effects of surface tension decrease and so does the rim flow rate.

As far as the rim velocity is concerned, it is purely radial with values smaller than and proportional to the liquid sheet velocity (Fig. 17). The constant of proportionality depends on the angle of the liquid sheet $\theta$.

It has been assumed in several previous works that the velocity profile of liquid sheets formed by fan sprays is radial and with a uniform mean value given by the flow rate and the nozzle orifice area (Dombrowski and Hooper, 1962; Weihs, 1978). Results from simulations on industrial atomizers carried out in this work show that, as the flow leaves the nozzle, a *vena contracta* is formed

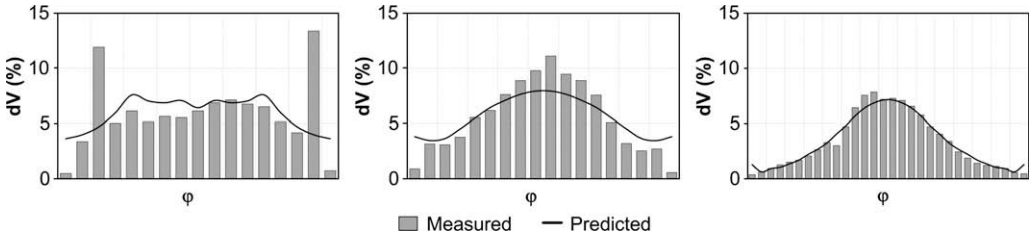


**Fig. 15.** Spatial pattern of $N_1$ (left), $N_2$ (center) and $N_3$ (right) at 3 bar.

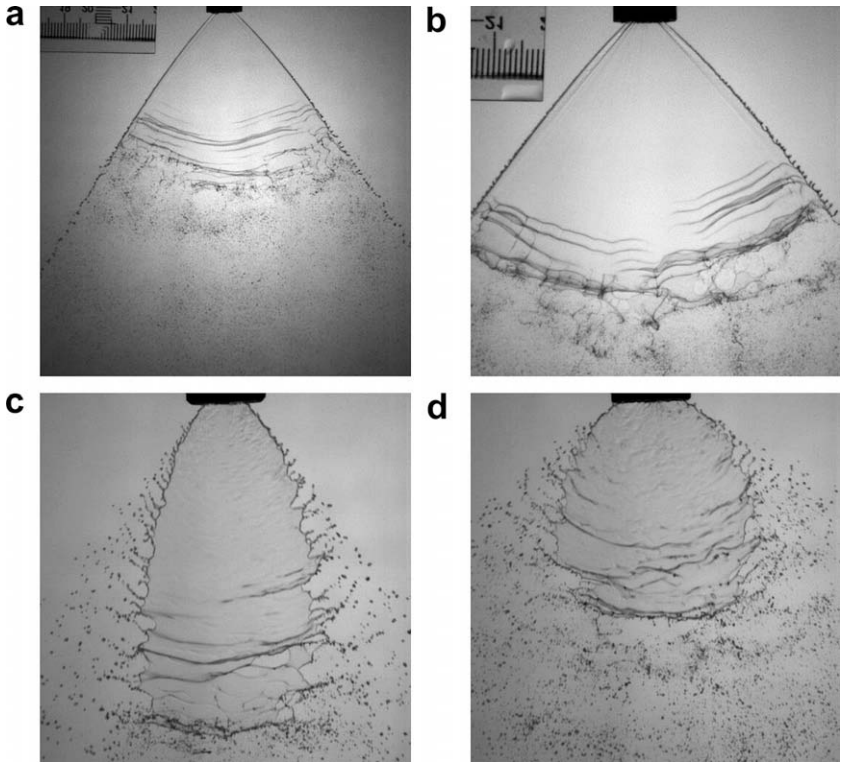


**Fig. 16.** High speed images of $N_1$ at 1 bar (a) and $N_1$ (b), $N_2$ (c) and $N_3$ (d) at 3 bar.

**Table 3**
Variation of $q_{RIM}/q_{TOTAL}$ with the radial coordinate.

| $r'/A^{1/2}$ | $N_1$ | | | | $N_3$ | | | |
|---|---|---|---|---|---|---|---|---|
| | 1 bar (%) | 2 bar (%) | 3 bar (%) | 4 bar (%) | 1 bar (%) | 2 bar (%) | 3 bar (%) | 4 bar (%) |
| 0.2 | 3.3 | 3.4 | 3.0 | 3.1 | 1.2 | 1.7 | 1.5 | 1.7 |
| 0.8 | 5.3 | 4.3 | 4.1 | 4.2 | 2.4 | 1.9 | 2.3 | 2.2 |
| 1.4 | 5.2 | 5.0 | 4.8 | 5.1 | 4.1 | 2.9 | 2.6 | 2.7 |
| 2 | 6.3 | 5.3 | 5.1 | 5.6 | 5.0 | 3.7 | 3.3 | 3.1 |

(Fig. 17). Then, the liquid sheet undergoes sudden area reduction leading to an increase in its velocity up to 45% depending on the geometry and the operating conditions. This fact has also been observed experimentally by Stetler et al. (2002).

Further downstream, once the liquid sheet is developed, its velocity magnitude becomes uniform and mainly radial. Nevertheless, this mean velocity is not the one given by the flow rate and the area of the outlet orifice, but larger due to the previous sudden cross-sectional area reduction. It should be underlined that, although the studied designs present different values of the discharge coefficient, the final velocity of the developed liquid sheet is very similar. A development region could then be defined where the liquid sheet is strongly influenced by the internal flow. This region, as depicted in Fig. 17, extends up to an approximate dimensionless radial coordinate of 0.4.

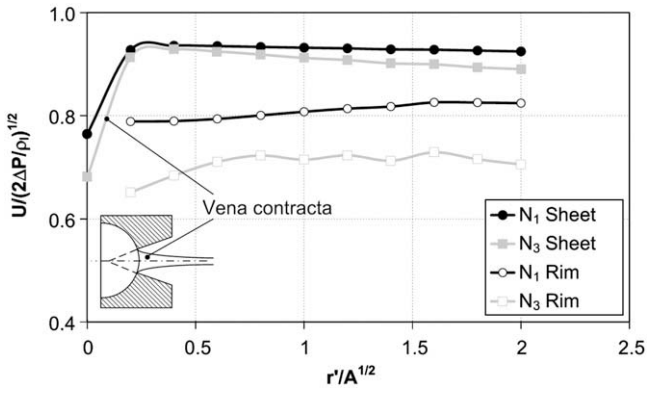


**Fig. 17.** Radial evolution of velocity magnitude for the liquid sheet and the rim.

Accepting the assumption of purely radial velocity of the liquid sheet, the growth of the rim is only due to surface tension (Clark and Dombrowski, 1971). However, studied atomizers produce a liquid sheet with both radial and tangential velocity components, adding another major contribution to the incoming flow rate of the rim.

Surface tension effects on the liquid sheet angle have been properly reproduced by the Continuum Surface Force model, as can be seen in Fig. 18. Although the results are not a contribution to the objective of this work, the use of a mathematical model allowed the study of the liquid sheet behavior in absence of surface tension, which is impossible to carry out in experimental tests. Simulations undertaken considering a zero-valued surface tension coefficient lead to a larger angle almost independent on the operating pressure. Additionally, and contrary to the results with non-

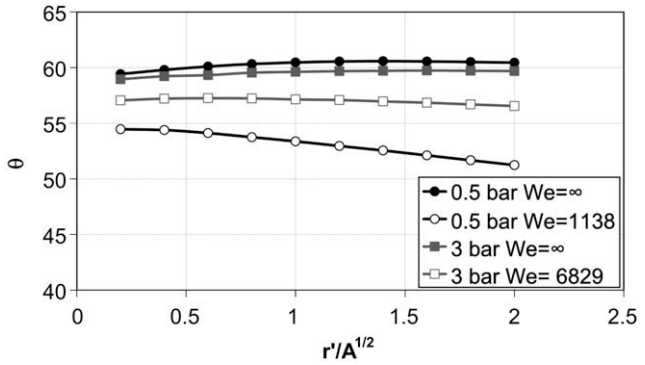


**Fig. 18.** Evolution of liquid sheet angle with the dimensionless radial coordinate for $N_3$. Surface tension effect.

zero surface tension, the liquid sheet angle did not decrease with the distance from the nozzle. It has also been observed that, according to what has been previously stated, an accumulation of liquid is formed at the free edge due to the tangential component of the velocity.

Contours of the tangential velocity component of $N_1$ and $N_3$ are depicted in Fig. 19. It can be observed that, although $N_1$ presents larger values for this magnitude at the outlet, downstream both nozzles present the same range of values and similar profiles. The maximum values are developed at the borders of the liquid stream at the region near the orifice; decreasing its value while moving downstream tending to a uniform profile. Thus its contribution to the rim flow rate will be larger at the region near the outlet and decrease with the distance from the nozzle.

To discern between both contributions and evaluate their relative influence on the growth of the rim, the analysis of the incoming flow rate of the rim has been carried out taking a differential element as represented in Fig. 20.

The flow rate increase throughout the differential element can be expressed as

$$q_{R2} = q_{R1} + \delta q_{R12} \tag{25}$$

where

$$\delta q_{R12} = \mathbf{u}_{Sheet} \cdot \boldsymbol{\delta S} \tag{26}$$

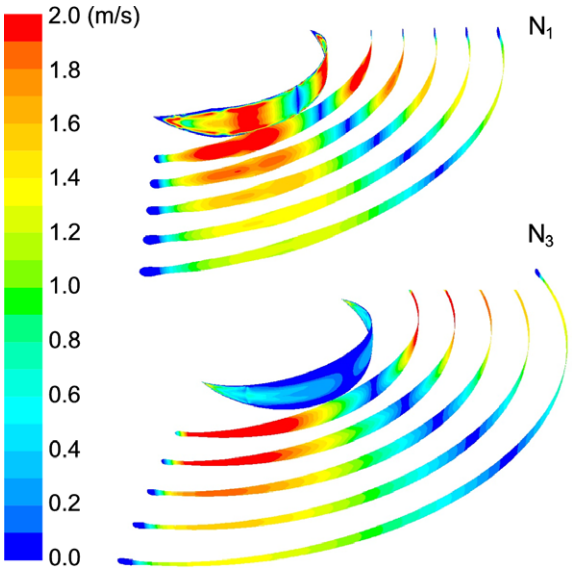


**Fig. 19.** Contours of tangential velocity (m/s) at 3 bar for surfaces of constant $r'/A^{1/2}$ for $N_1$ (above) and $N_3$ (below).

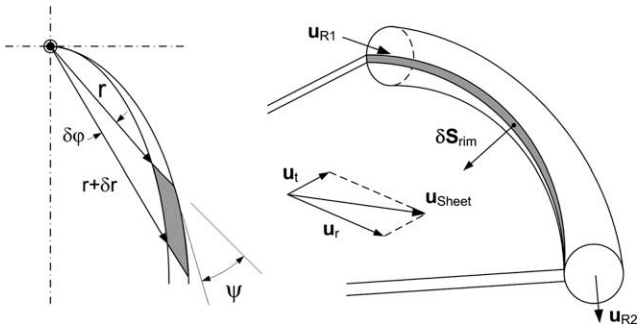


**Fig. 20.** Diagram of the rim incoming flow rate contributions.

is the incoming flow rate, which can be separated into two terms related to surface tension effects and the tangential component of the liquid sheet velocity, as follows:

$$\begin{aligned} \delta q_\sigma &= u_r \cdot \delta S \cdot \sin\psi \\ \delta q_t &= u_t \cdot \delta S \cdot \cos\psi \end{aligned} \tag{27}$$

being

$$\begin{aligned} \sin\psi &= \frac{r \cdot \delta\varphi \cdot 2h}{\delta S} \\ \cos\psi &= \frac{\delta r \cdot 2h}{\delta S} \end{aligned} \tag{28}$$

In the last expressions $\delta S$ stands for the length of the arc corresponding to the differential element and $\psi$ is the angle between the radial direction and the tangent to the rim. Values of the incoming flow rate, $h$ and $\delta S$, as well as the area-weighted averaged products $\overline{u_t \cdot \cos\psi}$ and $\overline{u_r \cdot \sin\psi}$, were obtained from the simulations at different distances from the orifice. Although the radial velocity component is always larger than the tangential, the small values of $\psi$ make their contribution to the incoming flow rate of the rim of the same order of magnitude (see Eq. (27)).

It is known that $N_3$ features a larger angle $\theta$ than $N_1$, leading to smaller $\delta\varphi$ for a certain $\delta r$. Taking into consideration that both nozzles give similar flow rates for a given operating pressure, posing a mass balance of the liquid sheet, one can conclude that $\delta S$ and $\psi$ are larger for $N_1$ than for $N_3$. Since $\psi = O(0)$, the term $\cos\psi$ is $O(1)$ and $\sin\psi$ is $O(\psi)$. Even though the contribution of the tangential velocity is almost the same for both nozzles, the larger the angle of the liquid sheet ($\theta$) the lower the contribution of surface tension effects to the growth of the rim. Therefore, liquid sheets with larger angles tend to develop thinner rims.

Posing the rim instability problem as the disintegration of a liquid jet, the thinner rim of nozzle $N_3$ would have a shorter characteristic breakup time than those of $N_1$ and $N_2$ and hence, an earlier disintegration into droplets. If this was the only mechanism governing the destabilization of the rim, one could conclude that nozzles with the same liquid sheet angle should present similar rim behavior. However, as can be seen in Fig. 16, the destabilization of the rims produced by $N_1$ and $N_2$, with similar angles, is quite different. High-speed imaging of the liquid sheets formed by these nozzles reveal that, while $N_1$ presents a smooth surface free of turbulent perturbations, $N_2$ and $N_3$ have a highly disturbed surface, even near the outlet of the atomizer. It has also been observed that these turbulent disturbances impact on the already disturbed rim, causing its early atomization and enhancing liquid sheet breakup. This effect was also observed by Bremond and Villermaux (2006) when inducing perturbations in the liquid sheet with an external device. So, it could be concluded that, together with the liquid sheet angle, turbulence has a significant influence on the behavior of the rim produced by the nozzles under study.

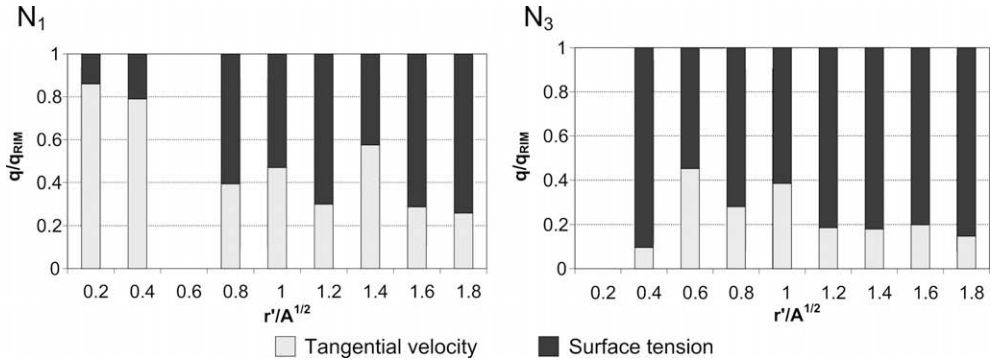


**Fig. 21.** Ratio between tangential velocity and surface tension contribution to the rim incoming flow rate.

It should be pointed out that, mainly in $N_3$, the estimation of $\psi$ is critical, presenting significant variations due to discretization. Since the coordinates of the rim boundary were taken from the discrete domain, for some differential elements negative values of $\delta\varphi$, and thus of $\psi$, were obtained. However, since the main objective of this analysis was to prove that the effects of both contributions were comparable in magnitude, the exact values of the flow rate were not considered as important as the qualitative conclusions obtained. Fig. 21 depicts the ratio between the incoming flow rate due to surface tension and the one from the tangential velocity for $N_1$ and $N_3$. Missing columns correspond to non-logical values of $\psi$ due to discretization, leading to incorrect flow rates. It can be seen that, near the orifice, the incoming flow rate of the rim for $N_1$ is mainly due to tangential velocity. While moving downstream, the contribution of surface tension gains relative importance, as the magnitude of tangential velocity decreases.

Regarding turbulence modeling, and as previously stated, simulations of $N_1$ have been undertaken adopting different models, namely: k-ε Standard, RNG and Realizable and k-ω SST. It should be stressed that, due to the larger discretization error of the model considering the round edge, calculations for this discussion have been carried out neglecting this feature. However, it will be seen that, out of the nozzle outlet, the round edge has not a major influence on turbulent magnitudes or velocity profiles. As for the verification of the mathematical model, due to the resemblance between the geometries of all three designs, analogue studies for $N_2$ and $N_3$ have not been carried out.

It is known that all models based on the Boussinesq hypothesis present certain limitations when dealing with flows with large rapid extra strains, providing overpredicted turbulent kinetic energy. Although the k-ε RNG model contains a strain-dependent correction term in the ε equation which is supposed to correct this limitation, as noticed by Hanjalic (2004), this term does not account for the sign of the strain.

Very similar values of the most characteristic integral magnitudes of the problem have been obtained from all the turbulence models considered (Table 4). Results obtained from k-ε Standard model present slight differences, featuring a larger thickness factor and discharge coefficient, which is consistent with the results obtained by Yeh (2005). In general, it can be stated that the mean flow of the liquid sheet is not much affected by turbulence modeling. This is a positive conclusion from the manufacturer point of view, who is mainly interested on the characterization of the liquid sheet.

**Table 4**
Values of characteristic magnitudes of the problem for the turbulence models employed.

| | k-ε | | | k-ω SST |
|---|---|---|---|---|
| | Standard | RNG | Realizable | |
| $\theta$ (°) | 45.53 | 45.39 | 46.21 | 46.40 |
| $C_D$ | 0.687 | 0.659 | 0.659 | 0.652 |
| $K$ (mm$^2$) | 0.305 | 0.278 | 0.279 | 0.258 |

Fig. 22 illustrates the profiles of dimensionless $Z$-velocity, turbulent intensity and viscosity ratio for the different turbulence models considered. Results from the Realizable model have been omitted due to their resemblance with the RNG model.

Velocity profiles corresponding to the nozzle tip are almost identical for all the models. At the external region, the velocity predicted for the liquid sheet features a uniform profile along its thickness. In this aspect, the k-ε Standard model gives a thicker liquid sheet with a slightly lower average velocity. The most important differences have been observed regarding the depth of the air entrainment region (Fig. 22). This part of the air flow influenced by the liquid sheet is a key issue for the subsequent analysis of instability and break up as well as for the spray dynamics. It can be seen that this region grows almost linearly for all the models, being larger for all k-ε models than for the k-ω SST.

With regard to the turbulent viscosity, the expression employed for its calculation differs among the models under study. The definition of turbulent viscosity at the k-ω SST, which introduces a limiter to prevent its excessive growth, leads to a sudden extinction of this magnitude and turbulent kinetic energy production inside the nozzle's tip, where a turbulent level increase should be expected. Although the k-ε RNG accounts for the turbulent viscosity through a differential equation to handle low Reynolds number flows, the turbulent Reynolds number throughout the domain yields an expression which is analogous to that of the k-ε Standard, with a value for the $C_\mu$ coefficient of 0.0845 instead of 0.09. So the differences between the turbulent viscosity given by the RNG and the Standard k-ε models do not rely on the expression itself but on the data with which it is calculated. The additional source term of the epsilon equation in the RNG k-ε model gives a smaller destruction of ε for rapidly strained flows and, consequently, lower values of k and $\mu_t$ than the Standard k-ε.

One of the main fronts in turbulence modeling is the search of representations able to guarantee realizability of the solution. In this aspect, none of the models considered provides a completely realizable solution, being the k-ε RNG the one giving the smallest non-realizable region from all the k-ε models studied. Although the k-ω SST model is even more realizable than the k-ε RNG, this is due to the turbulent viscosity limiter which, as stated above, goes against the physics of this particular flow. The authors have observed that the lack of realizability is related to high values of the ratio between production and dissipation of turbulent kinetic energy.

Images (b) and (d) depicted in Fig. 16 make clear the existence of fundamental differences in the development of the liquid sheets from $N_1$ and $N_3$ and, consequently, in their respective flow magni-

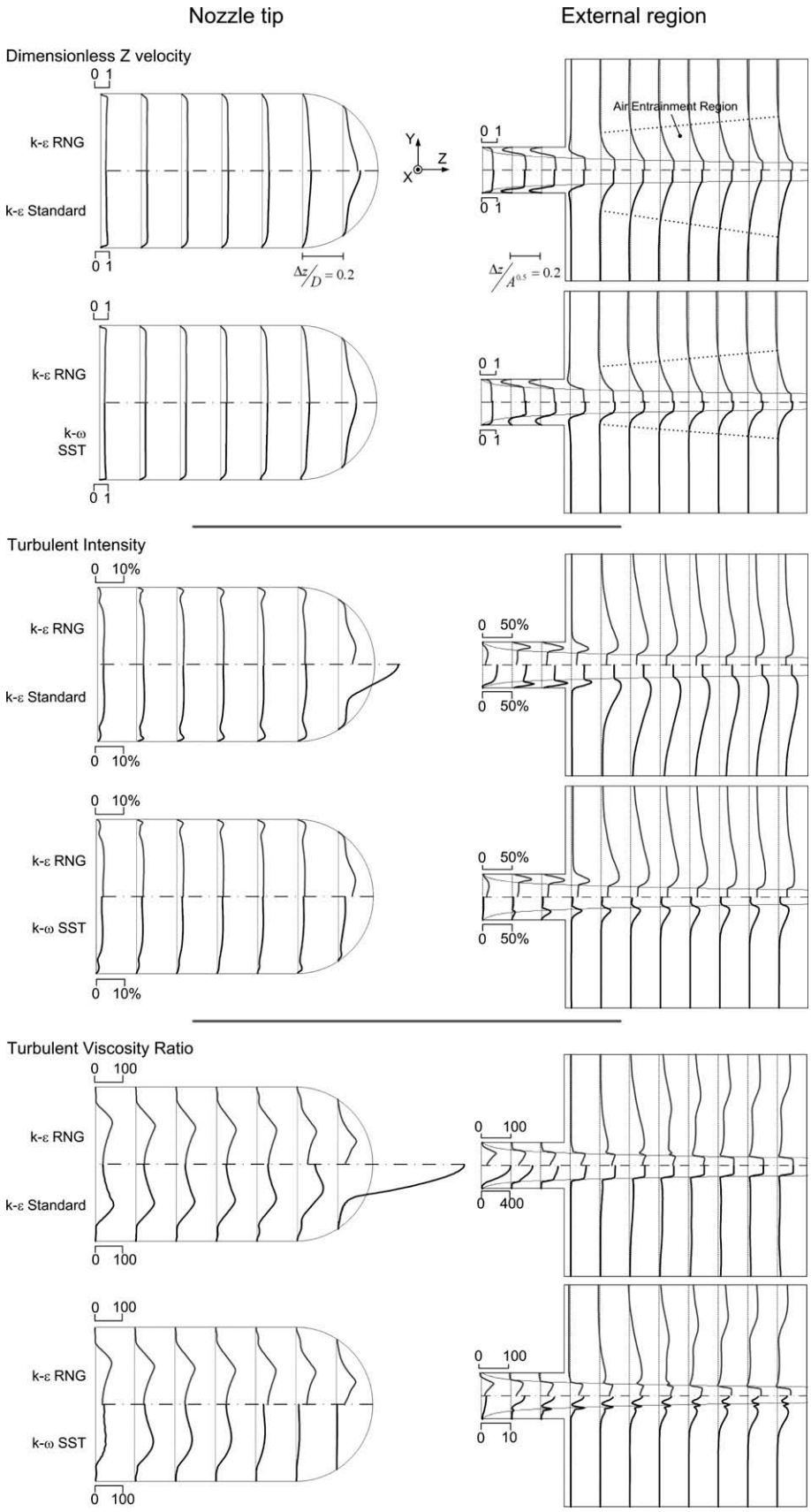


**Fig. 22.** Profiles of dimensionless *Z* velocity, turbulent intensity and turbulent viscosity ratio for the three turbulence models employed (please note that in some cases scales are different).

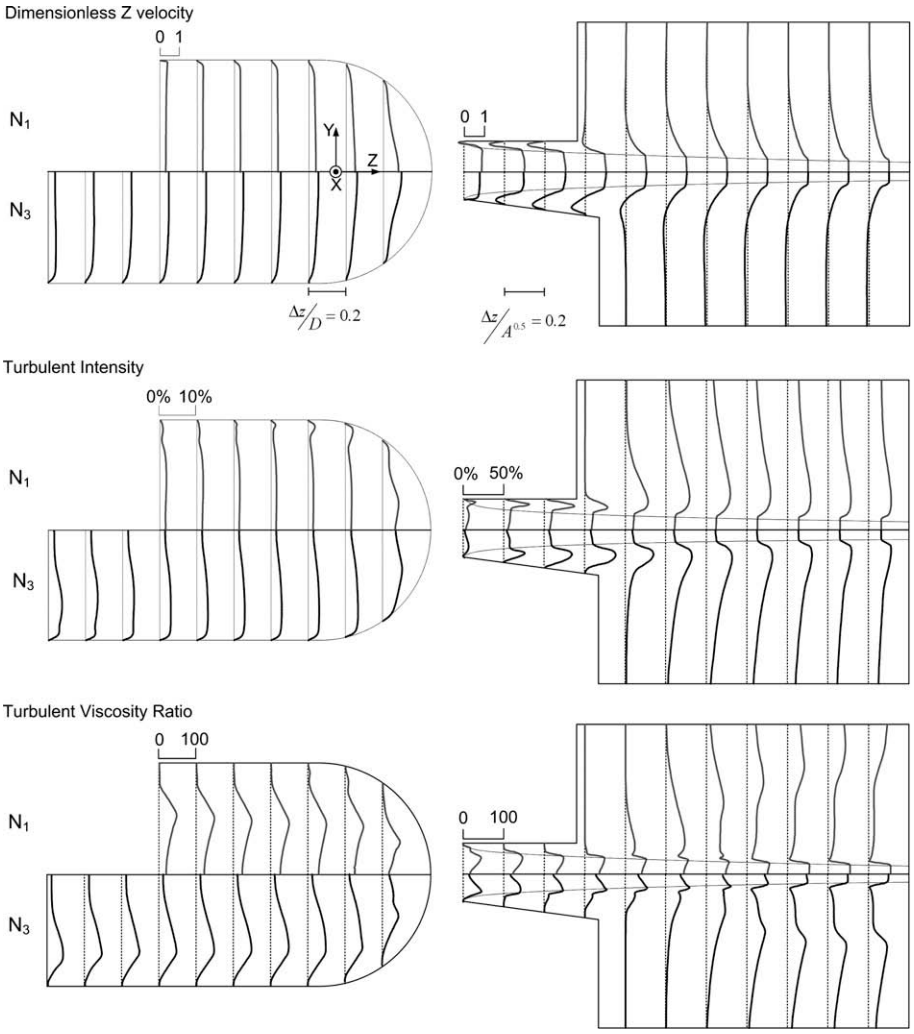


**Fig. 23.** Profiles of dimensionless *Z* velocity, turbulent intensity and turbulent viscosity ratio of $N_1$ and $N_3$ with the RNG k-ε model.

tudes. For this reason, a more extensive analysis of their velocity profiles and turbulent magnitudes has been considered of interest.

The profiles of dimensionless *Z* velocity, turbulent intensity and viscosity ratio for $N_1$ and $N_3$ are plotted in Fig. 23 These profiles correspond to the calculations adopting the RNG k-ε turbulence model. The flow enters the tip with larger turbulent kinetic energy for $N_3$ than for $N_1$ due to the sharp cross-section area reductions of the former.

The external shape of the nozzle appears to play an important role on the development of turbulence in the surrounding air, favoring the entrance and recirculation of the air flow and avoiding large pressure gradients.

Although near the outlet the turbulent intensity is not constant along the liquid sheet thickness, further downstream it becomes uniform and has almost the same value for both nozzles. The effect of the external shape also dilutes with the distance from the nozzle.

It should be mentioned also that, even though the round edge of $N_1$ has a strong influence on the discharge coefficient or other flow magnitudes at the very near field region of the outlet, further

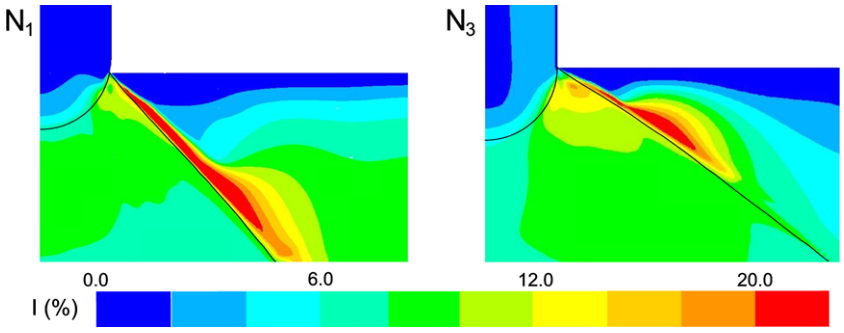


**Fig. 24.** Contours of turbulent intensity for $N_1$ and $N_3$ at 3 bar at the *XZ* symmetry plane.

downstream there is no substantial difference between the profiles of the plotted magnitudes with and without this feature.

However, these results do not elucidate the fundamental differences between the liquid sheets formed by these two designs. It is clearly distinguishable from pictures (b) and (d) of Fig. 16 that the border of $N_3$ is highly disturbed and rapidly disintegrates into droplets enhancing the breakup of the liquid sheet itself. Alternatively, the border developed by $N_1$ thickens and follows the mechanisms of destabilization and breakup typical from a jet, independently of the liquid sheet. This fact, together with observations about the rim disintegration previously described, motivated the representation of turbulent intensity at the *XZ* symmetry plane for both designs (Fig. 24). It can be seen that, although the air surrounding the liquid sheet from $N_1$ has a larger turbulent intensity than that of $N_3$, values of this magnitude inside the liquid sheet of the latter are larger and concentrated in the border, which may lead to its prompt destabilization and breakup.

## 8. Conclusions

In this paper, CFD techniques have been used in fan spray nozzles' characterization providing accurate and very useful data about the flow taking place inside the tip and the development of the liquid sheet for three different designs. The mathematical model has been defined, verified and subsequently validated. Model validation has been carried out by assessing its ability to predict several experimentally measured flow features, which were measured in several units of every design to avoid dependences on manufacturing defects.

The importance of accurate knowledge of nozzle geometry has been demonstrated through the changes in nozzle performance produced by the presence of a round edge at the orifice of design $N_1$. The addition of this feature to the geometry was found to be decisive for the correct prediction of the discharge coefficient.

The experimental technique employed for the validation of the thickness factor, based on interferometry, has turned out to be extremely sensitive to the presence of perturbations on the liquid sheet surface.

Regarding the spatial distribution of the spray, although it is highly influenced by the processes of primary and secondary breakup, reliable results have been obtained. This has allowed model validation and has also strengthened mathematical modeling by means of CFD techniques as a useful tool for nozzle design.

A development region has been defined near the outlet of the nozzle where a *vena contracta* is formed leading to an acceleration of the fluid. This fact entails a radical change in the traditional assumption that the liquid sheet velocity is uniform, constant and given by the flow rate and the cross-sectional area of the outlet.

The velocity profile of the atomizers under study presents a tangential component which contributes to the growth of the rim at the same grade than surface tension along the region near the outlet of the atomizer, especially in $N_1$. Both contributions, but mainly surface tension effects, are dependent on the angle of the liquid sheet; so that the larger the angle, the lower the incoming flow rate to the rim.

The use of different turbulence models has revealed no relevant differences in the basic integral magnitudes of the liquid sheet flow, although a significant influence has been observed regarding the depth of the air entrainment region all k-ε models provide similar results while the k-ω features a thinner shear layer. Nevertheless, with a view to future modeling of the instability and breakup process, the structure of the shear layer produced and the effect of turbulent scales through the term $\overline{\alpha' u_i'}$ both in the liquid and the gas phase flow should be taken into account and analyzed in depth.

## Acknowledgements

This research was partially funded by Eusko Jaurlaritza-Gobierno Vasco, Spain through grants UE-2004-14, EC2006-11 and PI2007-13, by the Universidad de Navarra through the PIUNA program and, finally, by the Diputación Foral de Gipuzkoa. The authors would like to thank Goizper-Olaker and especially Iñigo Iparragirre for their invaluable help. The financial support of Cátedra Fundación Antonio Aranzábal–Universidad de Navarra is also gratefully acknowledged. Finally, the authors are very thankful for all the fruitful suggestions of the reviewers.

## References

Barth, T.J., Jespersen, D., 1989. The design and application of upwind schemes on unstructured meshes. Technical Report AIAA-89-0366, AIAA 27th Aerospace Sciences Meeting, Reno, Nevada.

Brackbill, J.U., Kothe, D.B., Zemach, C., 1992. A continuum method for modeling surface tension. J. Comput. Phys. 100, 335–354.

Bremond, N., Villermaux, E., 2006. Atomization by jet impact. J. Fluid Mech. 549, 273–306.

Bush, J.W.M., Hasha, A.E., 2004. On the collision of laminar jets: fluid chains and fishbones. J. Fluid Mech. 511, 285–310.

Chen, H.C., Patel, V.C., 1988. Near-wall turbulence models for complex flows including separation. AIAA J. 26 (6), 641–648.

Choo, Y.J., Kang, B.S., 2001. Parametric study on impinging-jet liquid sheet thickness distribution using an interferometric method. Exp. Fluid 31, 56–62.

Clanet, C., Villermaux, E., 2002. Life of a smooth liquid sheet. J. Fluid Mech. 462, 307–340.

Clark, C.J., Dombrowski, N., 1971. The dynamics of the rim of a fan spray sheet. Chem. Eng. Sci. 26, 1949–1952.

Dombrowski, N., Hasson, D., Ward, D.E., 1960. Some aspects of liquid flow through fan spray nozzles. Chem. Eng. Sci. 12, 35–50.

Dombrowski, N., Hooper, P.C., 1962. The effect of ambient density on drop formation in sprays. Chem. Eng. Sci. 17, 291–305.

Fraser, R.P., Eisenklam, P., Dombrowski, N., Hasson, D., 1962. Drop formation from rapidly moving liquid sheets. A.I.Ch.E. J. 8 (5), 672–680.

Gueyffier, D., Li, J., Nadim, A., Scardovelli, R., Zaleski, S., 1999. Volume of Fluid interface tracking with smoothed surface stress methods for three-dimensional flows. J. Comput. Phys. 152, 423–456.

Hagerty, W.W., Shea, J.F., 1955. A study of the stability of plane fluid sheets. J. Appl. Mech., 509–514.

Hanjalic, K., 2004. Closure Models for Incompressible Turbulent Flows, Von Karman Institute Lecture Series Turbulence 2004. Von Karman Institute, Rhode-Saint Genese, Belgium.

Harlow, F.H., Welch, E., 1965. Numerical calculation of time-dependent viscous incompressible flow of fluids with free surface. Phys. Fluid 8, 2182.

Herrmann, M., 2002. An Eulerian level-set/vortex-sheet method for two-phase interface dynamics. In: Annual Research Briefs, C.f.T. Research, Standford University, pp. 185–196.

Hirt, C.W., Nichols, B.D., 1981. Volume of Fluid (VOF) method for the dynamics of free boundaries. J. Comput. Phys. 39, 201–225.

Ibrahim, E.A., 1997. Effect of velocity profile on liquid sheet instability. Chem. Eng. Sci. 52 (23), 4419–4422.

Jeandel, X., Dumouchel, C., 1999. Influence of the viscosity on the linear stability of an annular liquid sheet. Int. J. Heat Fluid Flow 20 (5), 499–506.

Kader, B., 1981. Temperature and concentration profiles in fully turbulent boundary layers. Int. J. Heat Mass Transfer 24 (9), 1541–1544.

Klein, M., 2005. Direct numerical simulation of a spatially developing water sheet at moderate Reynolds number. Int. J. Heat Fluid Flow 26, 722–731.

Lafaurie, B., Nardone, C., Scardovelli, R., Zaleski, S., Zanetti, G., 1993. Modelling merging and fragmentation in multiphase flows with SURFER. J. Comput. Phys. 113, 134–147.

Lakehal, D., Meier, M., Fulgosi, M., 2002. Interface tracking towards the direct simulation of heat and mass transfer in multiphase flows. Int. J. Heat Fluid Flow 23, 242–257.

Lan, H., Friedrich, M., Armaly, B.F., Drallmeier, J.A., 2008. Simulation and measurement of 3D shear-driven thin liquid film flow in a duct. Int. J. Heat Fluid Flow 29, 449–459.

Launder, B.E., Spalding, D.B., 1972. Lectures in Mathematical Models of Turbulence. Academic Press, London, England.

Lefebvre, A.H., 1989. Atomization and Sprays. Hemisphere Publishing Corp., USA.

Leonard, B.P., 1991. The ULTIMATE conservative difference scheme applied to unsteady one-dimensional advection. Comput. Method Appl. Mech. Eng. 88, 17–74.

Liovic, P., Lakehal, D., 2006. Multi-physics treatment in the vicinity of arbitrarily deformable gas–liquid interfaces. J. Comput. Phys. 222, 504–535.

Mehring, C., Sirignano, W.A., 1998. Nonlinear capillary wave distortion and disintegration of thin planar liquid sheets. J. Fluid Mech. 388, 69–113.

Menard, T., Tanguy, S., Berlemont, A., 2007. Coupling level set/VOF/ghost fluid methods: validation and application to 3D simulation of the primary break-up of a liquid jet. Int. J. Multiphase Flow 33 (5), 510–524.

Menter, F.R., Kuntz, M., Langtry, R., 2003. Ten years of experience with the SST turbulence model. Turbulence Heat Mass Transfer 4, 625–632. Begell House Inc.
Muzaferija, S., Peric, M., 1998. Computation of free-surface flows using interface-tracking and interface-capturing methods. In: Mahrenholtz, O., Markiewicz, M. (Eds.), Nonlinear Water Wave Interaction. Computational Mechanics Publications, Southampton, UK, pp. 59–100.
Nardone, C., Scardovelli, R., Zaleski, S., Zanetti, G., 1994. Modelling merging and fragmentation in multiphase flows with SURFER. J. Comput. Phys. 113, 134–147.
Ohnesorge, W., 1936. Formation of drops by nozzles and the breakup of liquid jets. Z. Angew. Math. Mech. 16, 355–358.
Patankar, S.V., 1980. Numerical Heat Transfer and Fluid Flow. Hemisphere, Washington, DC.
Patankar, S.V., Spalding, D.B., 1972. A calculation procedure for heat, mass and momentum transfer in three-dimensional parabolic flows. Int. J. Heat Mass Transfer 15, 1787.
Rayleigh, L., 1878. On the instability of jets. Proc. Lond. Math. Soc. 10, 4–13.
Richardson, L.F., 1927. The deferred approach to the limit. Trans. R. Soc. Lond. Ser. A 226, 299–361.
Rivas, A., Sánchez, G., Estévez, A., Ramos, J.C., 2005. Improving the design of fan spray atomizers through Computational Fluid Dynamics Techniques. In: 20th ILASS – Europe Meeting.
Roache, P.J., 1998. Verification of codes and calculations. AIAA J. 36, 339–342.
Roache, P.J., 1994. Perspective: a method for uniform reporting of grid refinement studies. J. Fluid Eng. 116, 405–413.
Ryskin, G., Leal, L.G., 1984. Numerical solution of free-boundary problems in fluid mechanics. Part 2. Buoyancy-driven motion of a gas bubble through a quiescent liquid. J. Fluid Mech. 148 (19).
Schegk, C., Löffler, F., Umhauer, H., 1985. Drop-size distributions produced by flat-spray nozzles. Part. Charact. 3, 14–19.
Shih, T.H., Liou, W.W., Shabbir, A., Yang, Z., Zhu, J., 1995. A new k-ε eddy-viscosity model for high Reynolds number turbulent flows – model development and validation. Comput. Fluid 24 (3), 227–238.
Shirani, E., Jafari, A., Ashgriz, N., 2006. Turbulence models for flows with free surfaces and interfaces. AIAA J. 44 (7), 1454–1462.
Sirignano, W.A., Mehring, C., 2000. Review of theory of distortion and disintegration of liquid streams. Prog. Energy Combust. Sci. 26, 609–655.
Smith, R.W., Miller, P.C.H., 1994. Drift predictions in the near nozzle region of a flat fan spray. J. Agric. Eng. Res. 59, 111–120.
Squire, H.B., 1953. Investigation of the instability of a moving liquid film. J. Appl. Phys. 4, 167–169.
Stetler, M., Brenn, G., Durst, F., 2002. The influence of viscoelastic fluid on spray formation from flat-fan and pressure-swirl atomizers. Atom. Sprays 12, 299–327.
Sussman, M., Smith, K.M., Hussaini, M.Y., Ohta, M., Zhi-Wei, R., 2007. A sharp interface method for incompressible two-phase flows. J. Comput. Phys. 221 (2), 469–505.
Taylor, F.R.S., 1960. Formation of thin flat sheets of water. Proc. R. Soc. Lond. 259, 1–17.
Weber, C., 1931. Disintegration of liquid jets. Z. Angew. Math. Mech. 11, 136–159.
Weihs, D., 1978. Stability of thin radially moving liquid sheets. J. Fluid Mech. 87, 289–298.
Yakhot, V., Orszag, S.A., 1986. Renormalization group analysis of turbulence. I. Basic theory. J. Sci. Comput. 1 (1), 3–51.
Yeh, Chun-Lang, 2005. Turbulent flow investigation inside and outside plain-orifice atomizers with rounded orifice inlets. Int. J. Heat Mass Transfer 41, 810–823.
Youngs, D.L., 1982. Time-dependent multi-material flow with large fluid distortion. In: Morton, K.W., Baines, M.J. (Eds.), Numerical Methods for Fluid Dynamics. Academic Press.
Zhou, Q., Miller, P.C.H., Walklate, P.J., Thomas, N.H., 1996. Prediction of spray angle from flat fan nozzles. J. Agric. Eng. Res. 64, 139–148.
Zhu, J., Sethian, J., 1992. Projection methods coupled to level set interface techniques. J. Comput. Phys. 100 (2), 435.